RESEARCH ARTICLE | MARCH 05 2024

Thermal, structural, and conductivity properties of As$_{14}$Sb$_{26}$S$_{(60-x)}$–(AgI)$_x$ chalcogenide glasses

Akila G. Prabhudessai ✉ ⓘ ; Sathravada Balaji; Sakthi Prasad; Shweta Chahal ⓘ ; Kaushik Biswas ⓘ ;
K. Ramesh ⓘ ; Anupama Yadav ⓘ ; Saswata Chakraborty; Partha Sarathi Kongar; Sayan Chatterjee;
Sutanu Dutta; Rana Dasgupta; Pratik Sarkar; K. Annapurna ✉ ⓘ

Check for updates

View Online   Export Citation
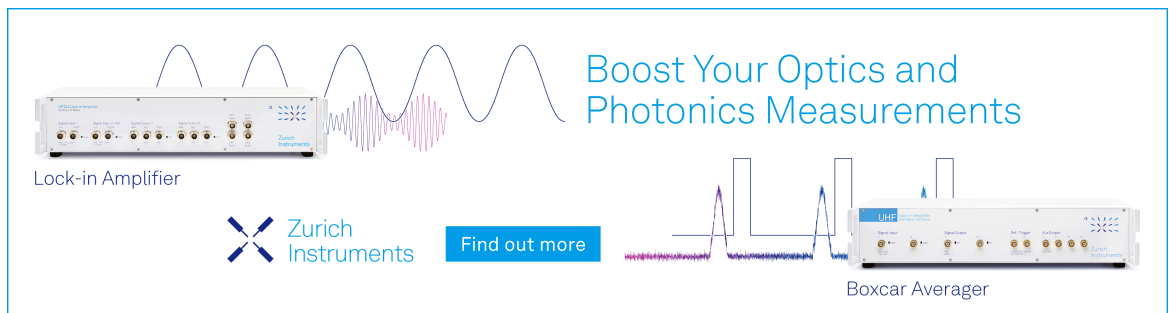
Thermal, structural, and conductivity properties of As$_{14}$Sb$_{26}$S$_{(60-x)}$–(AgI)$_x$ chalcogenide glasses

Akila G. Prabhudessai,[1,2,a] Sathravada Balaji,[3] Sakthi Prasad,[1,4] Shweta Chahal,[2] Kaushik Biswas,[1]
K. Ramesh,[2] Anupama Yadav,[1] Saswata Chakraborty,[1,4] Partha Sarathi Kongar,[1] Sayan Chatterjee,[1]
Sutanu Dutta,[5] Rana Dasgupta,[1] Pratik Sarkar,[1] and K. Annapurna[1,4,a]

AFFILIATIONS

[1]Specialty Glass Division, CSIR-Central Glass and Ceramic Research Institute, 196, Raja S. C. Mullick Road, Kolkata 700032, India
[2]Department of Physics, Indian Institute of Science, Bangalore 560012, India
[3]CSIR-National Environmental Engineering Research Institute, Hyderabad Zonal Centre, Tarnaka, Uppal Road, Hyderabad 500007, India
[4]Academy of Scientific and Innovative Research (AcSIR), CSIR-Human Resource Development Centre, (CSIR-HRDC) Campus, Postal Staff College Area, Sector 19, Kamla Nehru Nagar, Ghaziabad, Uttar Pradesh 201 002, India
[5]Bioceramics and Coatings Division, CSIR-Central Glass and Ceramic Research Institute, 196, Raja S. C. Mullick Road, Kolkata 700032, India

[a]Authors to whom correspondence should be addressed: akila912@yahoo.com and annapurnak@cgcri.res.in

ABSTRACT

The present work describes the preparation of a new series of chalcogenide glasses in an As$_{14}$Sb$_{26}$S$_{(60-x)}$ (AgI)$_x$ system intending to explore its thermal, structural, optical, mechanical, and electrical properties. The differential scanning calorimetry results of the studied glasses show the sharp decrease in glass transition temperature (T$_g$) with the successive incremental inclusion of AgI in the composition, implying the structural changes in the glass network. A thorough Raman analysis corroborates the occurrence of changes in the glass network due to the formation of AsI$_3$ units and Ag–S–As bonds with increasing AgI content. Also, structural changes can be reflected with the change in the optical bandgap (E$_g$) that was calculated using Tauc equations where it was found that E$_g$ is in harmony with the observed structural variations of glasses. The studied glasses possess a transmittance window ($\sim$0.68–12 μm) with transmittance above 60% in the mid-infrared region. These structural changes are closely related to the significant enhancement of conductivity of the present glasses from 10^{-8} to 10^{-6} S/cm at 373 K with a decrease in activation energies. Impedance spectra for the glass with highest AgI revealed the presence of two different relaxation processes. AC conductivity data followed an Arrhenius behavior as well as Jonscher's power law. The present work provides insights into glass network modifications due to silver iodide inclusion and its role in the enhancement of conductivity.

I. INTRODUCTION

Chalcogenide glasses (ChGs) have been studied for their mid-infrared (MIR) transparency, electrical properties, and flexible structure by many researchers from a long time.[1–8] In recent years, there has been a huge demand for portable energy devices, MIR lasers, photonics devices, MIR chemical sensors for detecting pollutants in air and water, and far-infrared (FIR) transparent materials for space applications to detect the possibility of extraterrestrial life by monitoring infrared signatures of ozone, water, and carbon dioxide (CO$_2$), leading to extensive studies of chalcogenide glasses.[5–7,9–13] Among all the chalcogens, sulfur-based glasses are mainly reported for their ionic conductivity and laser applications because the thermal and mechanical properties of most sulfide glasses are better than those of selenide or telluride glasses[2,13–16] Due to high glass transition temperature (T$_g$), transparency from visible to MIR ($\sim$10 μm), loose transport channels, and low binding energies, sulfur (S)-based glasses have been extensively studied for laser, photonics, and solid electrolyte applications.[2,4,14]

Sulfur-based glassy electrolytes, in particular, have attracted considerable interest due to their high polarization and the large ionic radius of sulfur S^{-2}, which enhance room temperature conductivity and ionic diffusion.[17] The major advantage of amorphous materials such as glasses is their ionic transport, which is driven without any grain boundary, leading to an increase in conductivity by several magnitudes compared to crystals.[17,18] In fact, the $LiI–Li_2S–GeS_2–Ga_2S_3$ chalcogenide glass is the best-known studied glass composition for solid electrolytes.[19,20] Many researchers have studied sulfur-based lithium halide glasses, and most of them have shown good conductivity at room temperature[20–22] However, glasses containing lithium iodide (LiI) pose challenges in terms of synthesis, chemical durability, volatility, and thermal stability.[19,23–26]

According to the studies available in the literature, silver-doped glasses usually exhibit higher conductivity as silver (Ag) ions are not held firmly in lattice sites or anion cages, thus having a great freedom of movement.[16,26] Silver doped in the form of AgI in ChGs helps to improve the glass-forming ability and optical properties as halide atoms (I^-) open up the network.[14,15,26] AgI enhances the conductivity of the glasses, as dopant salts usually expand the glass network, thus providing free volume for fast ion transport, which is associated with the large size of the anion (I^-).[27,28] Interestingly, AgI is also known as a super ionic conductor as its phase α-AgI has the highest ionic conductivity of 1 S/cm when it is thermodynamically stable above 147 °C.[16] At ambient pressure, the α-AgI phase is stable from 147 to 555 °C, which has a body-centered cubic structure and has the silver ions distributed randomly between 2, 3, and 4 coordinate sites.[29–32] At 147 °C, the phase transformation from α-AgI to low-temperature stable phase β/γ AgI occurs, making it difficult to work with α-AgI as it is not stable below 147 °C.[16] To date, only in oxide glasses and glass ceramics has α-AgI been stabilized at room temperature through the twin roller rapid quenching method.[16,33–36] At room temperature and normal pressure, two phases exist in silver iodide, the β phase (wurtzite structure) and the γ phase (sphalerite structure), where the β phase is claimed to be metastable.[37] Silver iodide (AgI)-doped glasses have been attracting many researchers as silver ions are known to exhibit a high conductivity of around 10^{-3} S/cm at room temperature.[14] The GeSbS and GeGaSbS or GaSbS[17,38,39] glass compositions are highly studied by doping silver iodide. Lin et al.[14] and Huang et al.[15] successfully synthesized glass by doping 70 mol. % of AgI without any crystalline phases. The glasses synthesized by Lin et al.[14] have displayed a high conductivity of around 9.18×10^{-3} S/cm at ambient temperature. Huang et al.[15] achieved high room temperature conductivity (10^{-3} S/cm) for 40 $(0.8Sb_2S_3–0.2Ga_2S_3)$–60 AgI sulfide glass. Most of the researchers have studied germanium- or gallium-based sulfide glasses, thus achieving good ionic conductivity at room and higher temperatures. However, AgI/AgCl-doped trivalent elements (As and Sb) containing sulfide glasses have been studied or explored by only a few researchers.[40,41] Among arsenic-containing glasses, As_2Te_3 glasses were studied by doping AgI,[42,43] and Kassem et al.[44] studied a CdTe-containing As_2Te_3 glass system doped with AgI. As_2Te_3 glasses have exhibited ionic–electronic mixed behavior,[43] whereas in AgI-doped As_2Se_3 glasses, the electronic process dominated the ionic conductivity.[45,46] As–Sb–S/As–Sb–S–I ChG glasses/thin films are explored by many for their structural, optical, and thermal properties, but conductivity properties are not studied much.[47–51] To the

best of our knowledge, no researchers have formulated and explored AgI-doped As–Sb–S systems. Previously, our group has investigated the effect of iodine addition on the optical, thermal, and structural properties of $As_{14}Sb_{26}S_{60}$ glasses by varying the As/Sb ratio.[52,53] Our studies have shown that As–Sb–S–I glasses exhibit favorable thermal and optical properties along with excellent glass-forming ability properties.[52,53] In this study, we incorporate AgI into the As–Sb–S system by replacing sulfur. While sulfur acts as a good glass former and enhances conductivity through the formation of Ag–S bonds, reducing its content increases the possibility of phase separation due to the presence of silver. It is worth noting that phase separation can occur in chalcogenide glasses doped with Ag and can result in non-homogeneous structures. This phenomenon has been observed in three- and four-component systems such as Ag–As–S, Ag–As–Se, and Ag–As–S–Se.[54–59] Phase separation appears as a result of the tendency of the system to reduce free energy by forming or separating it into two or more phases. Investigating phase separation is crucial for potential applications of these materials. Therefore, in this study, we examine the effect of silver iodide on the glass composition $As_{14}Sb_{26}S_{(60−x)}(AgI)_x$ (x = 2, 4, 6, 8, and 10 mol. %) in terms of structural modifications and its impact on thermal, optical, bulk mechanical, and electrical properties.

II. EXPERIMENTAL PROCEDURE

The chalcogenide glasses having the composition of $As_{14}Sb_{26}S_{(60−x)}(AgI)_x$ (x = 2, 4, 6, 8, and 10 mol. %) were synthesized by the melt quenching technique using raw materials such as arsenic (99.999%), sulfur (99.999%), and antimony (99.999%) from Alfa Aesar and silver iodide (99.9%) from Sigma Aldrich. The ampoules with appropriately weighed batches were evacuated under vacuum at 10^{-2} Pa followed by pre-heating and melting of batches at 750 °C in a rocking furnace for 16 h to homogenize the melt. The ampoules were quenched and then annealed for 2 h between 120 and 150 °C at a suitable temperature near T_g depending upon the composition. Annealed glasses were cut and polished according to the required dimension for further characterizations. The prepared glasses were labeled as G1–G5 (lowest to highest AgI content) for convenience. A photograph of all the studied glasses is shown in the inset of Fig. 1(a).

A. Material characterization

The x-ray diffraction (XRD) measurements for every sample in powder form were performed on an x-ray diffractometer (model: X'pert Pro MPD from Panalytical, Almelo, The Netherlands) using Ni-filtered CuK_α radiation of 1.5418 Å. The chemical composition of all the studied glasses was estimated using energy-dispersive x-ray spectroscopy (EDS) at an accelerating voltage of 20 kV equipped with a scanning electron microscope (SEM) (Carl Zeiss, Ultra 55, GEMINI, Germany). The densities of the bulk glasses were measured by applying Archimedes' buoyancy principle using toluene as an immersion liquid on a Mettler–Toledo digital mono-pan balance fitted with a density measurement kit. Differential scanning calorimetry (DSC) (model: LABSYS Evo; from Setaram, Caluire, France) studies were carried out from room temperature to 450 °C at the heating rate of 10 K/min. Raman spectra were recorded at room temperature using a Raman spectrometer (model: Labram, HR, 800
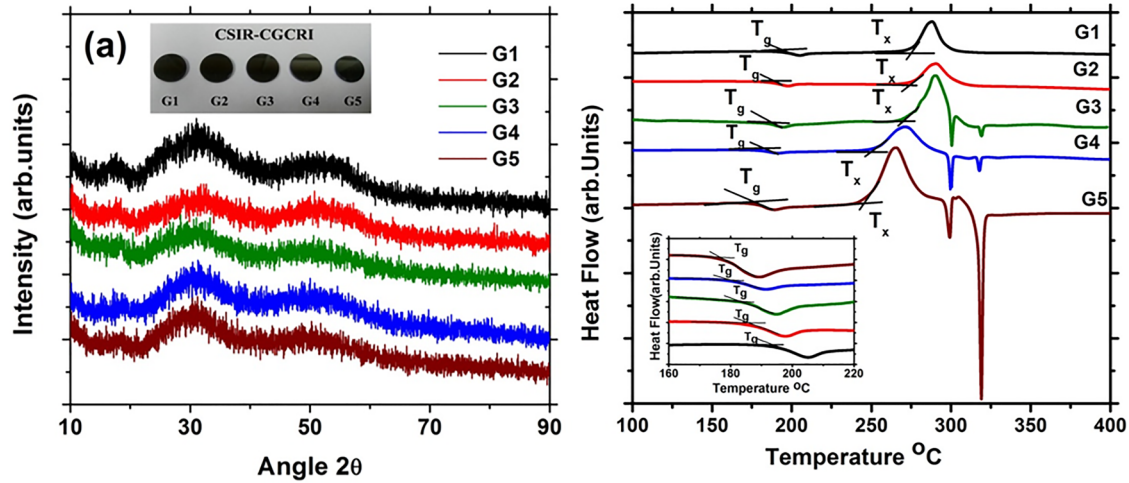
09 April 2024 09:31:30

FIG. 1. (a) XRD plot for all the glasses (inset: photograph of all the glasses). (b) DSC plots for all the studied glasses (inset: magnified view of Tg).

EV from Horiba, France) in the range of 120–400 cm^{-1} using a 785 nm laser diode as a source. The ultrasound velocity measurements at a 5 MHz frequency were carried out using an ultrasonic flaw detector (model: EPOCH-1000 from OLYMPUS, USA) to determine the bulk mechanical properties of glass.

1. Optical measurements

The optical properties were measured on the circular shaped samples of thickness 2 mm. The refractive index of all the samples was measured using a prism coupler (model: M2010 from Metricon USA) at a 1552 nm wavelength. The optical transmittance spectra were recorded in the spectral region in the range of 250–2500 nm using an ultraviolet–visible–near infrared spectrophotometer (UV–Vis–NIR spectroscopy) (model: Lambda 950, from Perkin Elmer, USA). The absorption coefficient (α) was calculated from the measured transmittance spectra of all glasses using equation[60] and is given in Eq. (1),

$$\alpha = \frac{2.303 \times A}{d},\qquad(1)$$

where A is the absorbance of the sample and d is the sample thickness or path length.

Optical bandgap calculations were carried out using the Tauc equation[60,61] and are given in Eq. (2),

$$\alpha h\nu = B(h\vartheta - E_g)^n,\qquad(2)$$

where E_g is the optical bandgap, B is the band edge parameter, n is an exponent that can take values of 1/2, 2, 1/3, or 3 depending upon the direct allowed, indirect allowed, direct forbidden, or indirect forbidden transitions, respectively. Bandgap (E_g) values were obtained from the extraction of linear fit and energy intercept. The infrared transmittance was measured for all the glass samples using a Fourier transform infrared (FTIR) spectrometer (model: Frontier from Perkin Elmer, USA) in the wavenumber range of 4000–400 cm^{-1}.

2. Electrical measurements

For impedance analysis, all the glass samples were uniformly cut into a circular disk shape with a thickness of ~1 mm. After cutting, glasses were polished to optical grade quality and then hand coated with high conductivity (volume resistivity = 0.0002 ohm cm) silver conductive paint (Pelco, Product No. 16062, Ted Pella Inc., USA). All the samples were cured for 48 h prior to the experiment. The conductivity measurements were carried out in the frequency range of 50 Hz–10 MHz using an LCR (L = inductance, C = capacitance, R = resistance) Hi-Tester model HIOKI-3532-50 (Hioki E. E. Corporation, Japan). A two-probe setup with test leads (parallel plate capacitor geometry) connected to a Test Fixture HIOKI-9262 was used to acquire the data. The temperature-dependent frequency characteristics of the glass samples were measured from RT to 100 °C with a 10 °C interval using a DPI-1200 high-temperature dry calibrator (Divya Process Instruments) with a temperature accuracy of ±1 °C. The sample bulk resistance, R_S, for the studied glasses at 100 °C was determined by extrapolating the semicircle to the Z′ (X axis) and the Nyquist plot for all the glasses. The AC conductivity (σ) at different temperatures can be calculated using Eq. (3),[17,62]

$$\sigma = \frac{d}{A \times R_S},\qquad(3)$$

where d is the sample thickness, A is the surface area, and R_S is the sample bulk resistance. EIS spectrum analyzer software was used for fitting the impedance data.[63]

III. RESULTS AND DISCUSSION

A. XRD and SEM-EDS analysis

Figure 1(a) shows the XRD plot for all of the glasses studied. The appearance of characteristic broad humps without any discrete diffraction peaks confirms the amorphous nature of the glasses.

TABLE I. Molecular weight (g/mol), density (g/cm³), glass transition temperature (T_g), crystallization onset temperature (T_x), crystallization peak temperature (T_c), melting temperature (T_m), and thermal stability factor (ΔT) of all the glasses. (All thermal parameters in °C.)

Sample code	Molecular weight	Density (±0.0006)	T_g (±2)	T_x	T_c	T_{m1}	T_{m2}	ΔT
G1	65.44	3.9256	192	280	290	423	…	88
G2	69.50	4.1110	187	273	288	400	…	84
G3	73.50	4.2895	180	261	285	302	322	81
G4	77.60	4.3697	177	252	270	299	319	75
G5	81.66	4.4380	172	240	265	298	320	68

EDS analysis was used to estimate the chemical composition of the bulk samples. The mole percent ratios for As, S, Sb, Ag, and I for all the glasses along with composition are given in Tables I and II in the supplementary material, along with standard error bars. The EDS analysis showed that there was minimal loss of iodine or silver content for all of the studied glasses, indicating that the composition of the final glasses remained almost intact. In addition to powder samples, bulk and polished samples of glass G1 (lower AgI content) and G5 (higher AgI content) were analyzed using SEM to study their microstructure. SEM scans were performed at ten different spots for both glasses. No grains, crystal formation, or inhomogeneity were observed in glass G1, even at higher magnifications. However, a non-uniform microstructure was observed at some spots in glass G5, which may be due to clustering or inhomogenities resulting from a higher AgI content. This was also confirmed using SEM mapping and EDS analsysis. All figures and minor details related to SEM-EDS, mapping, and analysis are given in Figs. S2–S4 in the supplementary material.

B. Physical and thermal properties

Table I lists the measured densities of the glasses. The density increases with an increase in silver iodide content, as it has a higher molar mass (234.77 g/mol) compared to the other elements in the glass system. Figure 1(b) shows the DSC plots for all the glasses, and Table I summarizes the obtained characteristic temperatures and thermal stability factor (ΔT). As silver iodide content increases from 2 to 10 mol. %, the glass transition temperature (T_g) decreases from 195 to 172 °C. This decrease is expected as iodine acts as a network terminator that forms many terminal bonds with silver, antimony, and arsenic, thus decreasing network connectivity or weakening the main structural units. The addition of metallic Ag⁺ may also be responsible for breaking (S–As–S/S–Sb–S) chains.[39]

The addition of AgI at the expense of sulfur content decreases the overall rigidity of the glass network. As silver increases, interconnected sulfur bonds are broken, thus decreasing overall thermal properties. Additionally, the crystallization onset temperature (T_x) decreased with an increase in silver iodide content. All glasses displayed a single crystallization peak or exothermic event. Glasses G3–G5 displayed double melting peaks, indicating that the presence of two crystallization peaks overlapped in one single peak. Glasses G1 and G2 displayed melting events beyond 400 °C and are given in Fig. S5(a) in the supplementary material. Melting events displayed by glasses G3 and G4, which were not visible clearly, are given in Fig. S5(b) in the supplementary material. The thermal

stability factor ΔT ranged between 88 and 68 °C and decreased with an increase in silver iodide. The decrease in sulfur content from 58 to 50 mol. % resulted in a decrease in bond energies as sulfur bonds have higher energies compared to halide bonds, which might be one of the strong reasons that accounted for the overall reduction in the glass transition temperature and thermal stability factor.

C. Optical properties

The UV–Visible–NIR and FTIR spectra of all studied glasses are shown in Figs. 2(a) and 2(b). Glasses have exhibited percent transmittance from 58% to 64% in the UV–VIS–NIR range and 60%–68% transmittance in the mid-infrared range with a transparency window beyond 11 μm. Major impurity peaks due to O–H, H_2O, and As–O bonds are observed in all the glasses. The impurity peak of As–O becomes sharper with an increase in AgI as halides are more prone to absorbing moisture. In the present glass series, the visible transmittance edge shifted to the higher energy side from G1 to G5, as shown in Fig. 2(b) with progressive inclusion of AgI.

1. Optical bandgap analysis

An indirect bandgap plot is given in Fig. 3(a), and values are mentioned in Table II. From Fig. 3(a), it can be observed that the bandgap is shifting toward a higher energy with an increase in silver iodide content. The bandgap shift can also be explained with the help of electronegativity and ionic radii of constituent elements. The electronegativities of arsenic, antimony, sulfur, silver, and iodine are 2.18, 2.05, 2.58, 1.93, and 2.66, respectively. Adding anions with a similar electronegativity to that of sulfur but larger ionic radii than those of sulfur (0.29), for example, can result in a high energy shift due to bandgap broadening caused by the large ionic radius (2.20).[64] Iodine, being the most electronegative element in the present glass system, plays an important role in trapping the electronic charges, thus resulting in extra electron energy levels in the bandgap.[65] This generates a larger optical bandgap; hence, a higher energy shift is observed with an increase in AgI content. As per Huang et al.,[15] the shortwave absorption edge (λ_{vis}) is also attributed to the electrical transition between a valence band and a conduction band. This phenomenon can be attributed to the addition of I⁻ with a lower polarizability (7.1×10^{-24} cm³) than that of S^{2-} (10.1×10^{-24} cm³).[15] The low polarizability of I⁻ results in an increase in the bandgap between the valence band and the conduction band. It is well known that the optical bandgap is not only influenced by chemical composition, but structural arrangement also plays an important role. The variation in S or AgI results in a change of bond angle or bond length, which
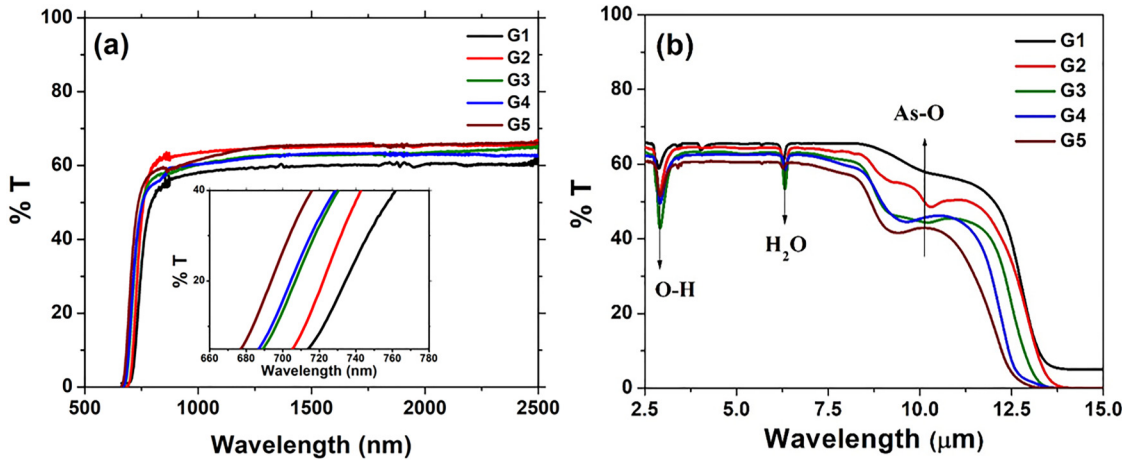
09 April 2024 09:31:30

FIG. 2. (a) UV–VIS–NIR spectra for all studied glasses (inset: magnified view of a shorter wavelength cutoff). (b) FTIR spectra for all studied glasses.

changes the glass matrix by their distribution in the entire network. As AgI enters the As–Sb–S glass network, it breaks As–S or Sb–S bonds and forms Ag–S bonds. As expected, there should be a red/lower energy shift in the visible bandgap, but iodine decreases the delocalization of non-binding electrons, which are in the form of lone pairs that are present in sulfur.[52]

In the chalcogenide glasses, the valence band is composed of lone pair electrons, whereas the conduction band is composed of empty orbits. Adding low-electronegativity atoms into the glass matrix increases the energy of the lone pair electrons and, in turn, expands the valence band width.[64] Therefore, adding the highly electronegative I^- (2.66) and low electronegative Ag^+ (1.93) elements into the glass network broadens the width of the forbidden band and consequently increases the optical bandgap.[64] For the studied glasses, an increase in AgI broadens the optical bandgap. In

fact, the influence of Ag and I atoms on the E_{opt} of glasses is totally opposite. The electrophilic character of I^- in the studied glasses plays beneficial roles in trapping lone pair electrons from S atoms and exciting the electrons from filled to empty states.[66] With an increase of AgI, the conduction band is hardly affected, but the valence band decreases. Consequently, the optical bandgap is broader and the effect of I supersedes that of Ag^{65} and E_{opt} decreases with an increase of Ag. This can be attributed to structural transformation. The Ag atoms enter into the glass structure and form their own connected structure.[66,67]

2. Refractive index and other optical parameters

For all the studied glasses, the refractive index was measured at a 1552 nm wavelength laser and is given in Table II. The
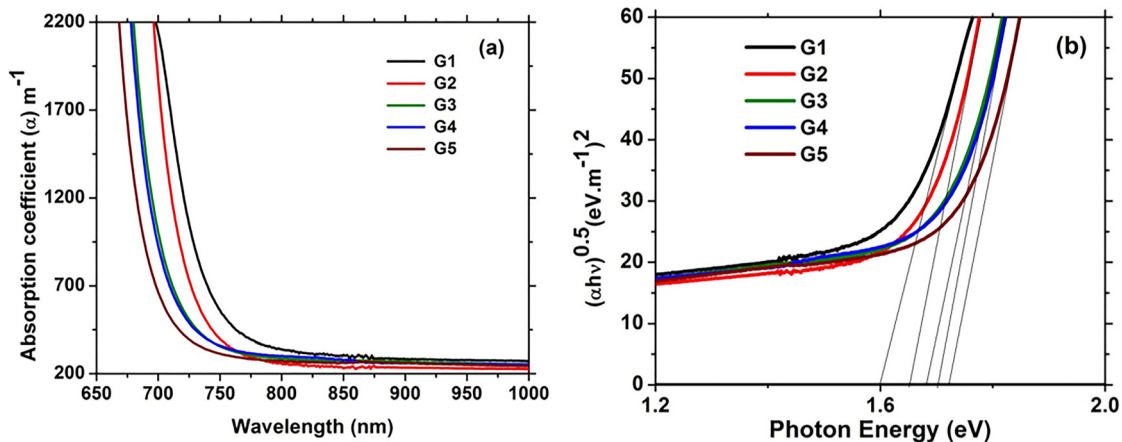

FIG. 3. (a) Absorption coefficient for all the studied glasses. (b) Indirect bandgap for all the studied glasses.

TABLE II. Measured refractive index (n) (at = 1552 nm), density (g/cm^3), molar volume (V_m, cm^3/mol^{-1}), molar refraction (R_m, cm^3/mol^{-1}), electronic polarizability ($\alpha_p \times 10^{-24}$ cm^3) (Clausius Mossotti equation), ($\alpha_m \times 10^{-24}$ cm^3) (Lorentz–Lorenz equation), and measured indirect energy gap (E_g, eV) from UV–Visible spectra of the prepared glass samples.

Glass code	n (±0.0005)	Toluene (±0.0006)	V_m	R_m	α_p (Clausius–Mossotti equation)	α_m (Lorentz–Lorenz equation)	E_g (eV) (indirect bandgap)
G1	2.7110	3.9256	16.67	11.32	5.00	4.49	1.62
G2	2.7021	4.1110	16.90	11.45	5.07	4.56	1.65
G3	2.7001	4.2895	17.15	11.61	5.14	4.61	1.68
G4	2.6643	4.3697	17.76	11.90	5.28	4.72	1.70
G5	2.6625	4.4380	18.40	12.33	5.47	4.89	1.72

refractive index has shown a decrease with an increase in silver iodide. The molar volume was calculated using the density and molecular weight. The molar refraction was calculated using the Lorentz–Lorenz equation[68] [Eq. (4)]. The Lorentz–Lorenz equation gives the average molar refraction for isotropic substances, which include liquids, glasses, and cubic crystals,[68,69]

$$R_m = \left(\frac{n_0^2 - 1}{n_0^2 + 2}\right) \times V_m. \quad (4)$$

The average electronic polarizability can be calculated from the Lorentz–Lorenz equation by introducing the Avogadro's number and is given in Eq. (5),[68,69]

$$\alpha_m = \frac{3}{4\pi N_A} \times R_m. \quad (5)$$

Here, N_A denotes Avogadro's number, which corresponds to the number of polarizable ions per mole. The value of $3/4\pi N_A$ is
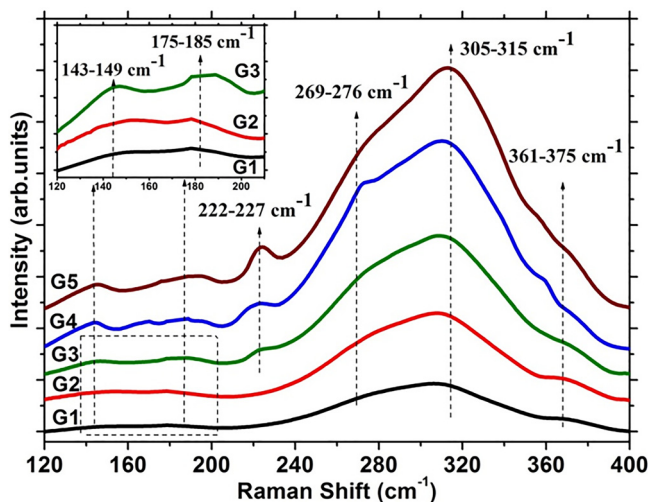

FIG. 4. Raman spectra for all the studied glasses (inset: magnified view of peaks between 120 and 200 cm^{-1}).

known as a constant in the Lorentz function. Electronic polarizability gives the magnitude of the electron response by applying the electromagnetic field to the electron clouds. After substituting, Eq. (5) becomes[68,69]

$$\alpha_m = \frac{R_m}{2.52}. \quad (6)$$

The Clausius–Mossotti relation is also used to know the electronic polarizability[69] and is given by Eq. (7),

$$\alpha_P = 0.395 \times \left(\frac{n^2 - 1}{n^2 + 1}\right) \times \left(\frac{M}{\rho}\right) \times 10^{-24}. \quad (7)$$

As clearly seen from Table II, the glass that contains the highest silver iodide (G5) has shown the highest, while G1, with the lowest AgI, has shown the lowest optical bandgap values among all other glasses in the series. The refractive index of all the glasses measured at 1552 nm is found to decrease with an increase in AgI content. This is quite an unusual trend as density values increase with the increase in iodine in glass composition and was also observed by Guo et al.[70] In glasses, the refractive index is generally determined by the molar refraction (R_m) and molar volume (V_m).[52] The larger R_m and smaller V_m give rise to a larger refractive index where V_m is related to density and R_m is related to ionic polarization. This implies that the higher the ionic polarization and density of glass, the higher the refractive index will be. In the studied glasses, both R_m and V_m increase as the addition of silver into the glass network contributes to the formation of cross-link structures. As more and more Ag$^+$ enters into the network, it breaks As–S/Sb–S bonds and cross-links Ag–S bonds, thus lowering the sulfur lone pairs. A decrease in lone pairs decreases the polarizability, and it results in a decrease in the refractive index. Interestingly, iodine forms terminal bonds with arsenic/antimony and enhances the molar volume. The introduction of iodine or any halide into the glass network usually decreases the refractive index and has been observed in different glass networks studied previously.[70–72] In the studied glasses, polarizability values calculated using Lorentz–Lorenz and Claussius–Mossotti equations have shown an increment. In the absence of silver iodide, sulfur forms bonds with arsenic and antimony, but when silver iodide enters the glass matrix, it not only terminates the bond but also enhances the molar volume, thus increasing the overall density as silver and

TABLE III. Raman shift along with peak assignments[15,16,28,47,49,50,53,73–83] in the prepared glasses (cm^{-1}).

Raman shift (cm^{-1})	Assignments
143–149	Glassy or vitreous Sb_2S_3
175–185	Sb–I vibrations in SbI_3 molecules
222–227	As–As homo polar bonds
269–276	$SbS_{3-x}I_x$ mixed structure
305–315	Asymmetric stretching vibrational modes of $AsS_{3/2}$ pyramids
361–370	AsS_3 pyramids connected by S–Ag–S linkage

iodine have opposite effects on the network.[66] Along with the refractive index, the optical bandgap shifted toward a lower wavelength, and as previously stated, iodine plays an important role here.

D. Raman spectroscopy

To elucidate the structural evolution of the studied glasses, Raman spectra (120–400 cm^{-1}) are recorded and are shown in Fig. 4. The deconvoluted Raman spectra are given in Fig. S6 in the supplementary material. We have reported and recorded spectra for all our glasses. The Raman peaks below 120 cm^{-1} were not taken into consideration due to the complications in identifying them accurately. Table III discusses the different types of bonds present in prepared glasses along with peak assignment and references.[50,73–81] The Raman spectra exhibited the peaks between 143 and 149, 175 and 185, 222–227, 269–276, 305–315, and 361–370 cm^{-1} depending upon the glass composition. All glasses in the series have shown a small peak around 143–149 cm^{-1}. This peak arises due to Sb–Sb bond vibrations in $SbSb_{3/3}$ structural groupings in glassy or vitreous Sb_2S_3 units[73,74] and was also observed in our previous studies on As–Sb–S–I chalcogenide glasses.[53] A small peak in the range of 175–185 cm^{-1} is exhibited by all the glasses, and its intensity increases with an increase in AgI content. This peak belongs to the low energy Sb–I bond vibrations in SbI_3 molecules.[53,76] The addition of silver iodide to the As–Sb–S glass network promotes the formation of Sb–S–I/Sb–I bonds, increasing the intensity of this bond as AgI increases. The peak near 222–227 cm^{-1} is observed only in those glasses that contain 6–10 mol. % of silver iodide and not in glasses with a lower

AgI concentration. In Ag_2S glasses, the Ag_2S modifier compensates the sulfur deficiency by converting bridging sulfur into terminal sulfur, thereby releasing its own sulfur species. However, this compensatory mechanism is not present in the case of AgI. Instead, the introduction of silver halides leads to increased chemical disorder, characterized by the formation of As–As homopolar bonds, which arise due to the absence of sulfur in AgI.[28,82] A shoulder peak near 265–276 cm^{-1} is observed in all the glasses and can be attributed to the formation of the $SbS_{3-x}I_x$ mixed structure, and a small enhancement can be observed with an increase in iodine.[15,16,45,78] The enhancement in the peaks of AsI_3 pyramidal and $SbS_{3-x}I_x$ units explains the decline in thermal properties as observed from Table I. An increase in iodine from 2 to 10 mol. % helps in terminating S–Sb–S/S–As–S bonds and promotes the formation of SbSI/AsSI bonds. Formation of these lower energy Sb–I/As–I terminal bonds also plays an important role in the red/blue shift in optical properties and also contributes toward the refractive index as mentioned in Secs. III C 1 and III C 2. The basic chemical reactions for the changes happening in As–Sb–S glasses after introducing silver iodide are given in Fig. S7 in the supplementary material.

The broad peak near 308–320 cm^{-1} is observed in all the glasses and is responsible for the vibrations of atomic pairs of antimony, arsenic, and sulfur in the structural units of SbS_3 and AsS_3 interconnected via two coordinated sulfur atoms.[79–81,83] The peak near 361–370 cm^{-1} is observed in all the glasses and a small enhancement can be seen with an increase in silver content. This peak is related to S–S–Ag bonds connecting AgS_3 pyramidal units.[79,81,83]

E. Bulk mechanical properties

In order to understand the changes in the glass network with an increase in AgI, bulk mechanical properties have been studied through ultrasonic velocities that are measured at room temperature. From measured ultrasonic velocities and density, values of longitudinal, shear, bulk, and Young's moduli were calculated by using standard formulas.[84,85] All the calculated parameters are listed in Table IV along with standard error bars. The addition of silver iodide decreased the ultrasonic velocities owing to network loosening by iodine. Though a decrease in velocities indicates the decline in rigidity of the glass network as well as elastic moduli, terminal bond formations/loosening of the network favors its conductivity. All the calculated values of elastic moduli have shown similar trends as velocities.

TABLE IV. Measured longitudinal velocity (V_L, m/s^{-1}) and shear velocity (U_S, m/s^{-1}) at a 5 MHz frequency, calculated longitudinal modulus (L, GPa), shear modulus (G, GPa), bulk modulus (K, GPa), and Young's modulus (E, GPa) of all prepared glasses.

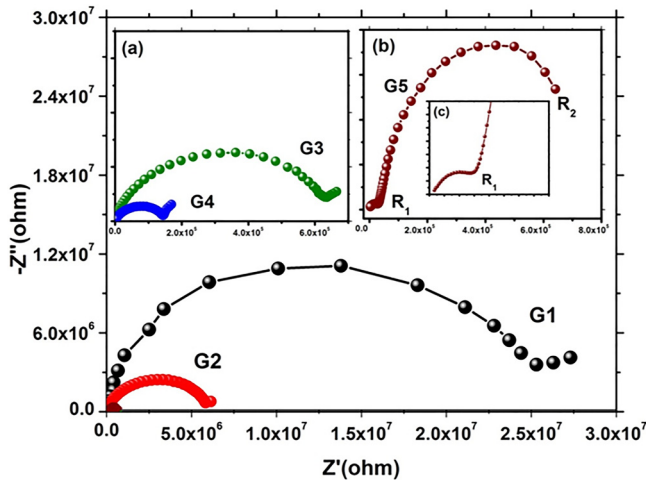| Sample code	G1	G2	G3	G4	G5
Longitudinal velocity (±6)	2658	2638	2546	2454	2310
Shear velocity (±3)	1484	1469	1377	1344	1308
Longitudinal modulus (±0.06)	28.95	28.80	27.57	26.06	24.18
Shear modulus (±0.04)	9.02	8.93	8.06	7.82	7.75
Bulk modulus (±0.02)	16.91	16.89	16.82	15.64	13.84
Young's modulus (±0.05)	22.98	22.78	20.86	20.09	19.60

09 April 2024 09:31:30

FIG. 5. Nyquist plot for all studied glasses at 100 °C. Inset: (a) magnified view Nyquist plots of glasses G3 and G4. (b) Magnified view of the Nyquist plot for glass G5. (c) Magnified view of the Nyquist plot at the higher frequency side of glass G5.

F. AC conductivity by impedance spectroscopy

Impedance spectroscopy is a widely used technique that employs the creation of an equivalent electric circuit model, whose elements consistently represent the electrical properties of the material from the aspect of physico-chemical characteristics of its structure.[86,87] In impedance spectroscopy, the representation of impedance (resistance and reactance) as a function of frequency is represented by using the Nyquist plot, which is a complex plane representation. Here, impedance is plotted as a complex number, with the real part of impedance on the x axis and the imaginary part on the y axis. This technique has proven to be successful in the characterization of high-resistant materials such as glasses, whether they are composed of a homogeneous or a heterogenic structure.[8,86,87] The sample bulk resistance, R_S, for glasses at 373 K G1–G4 was determined by extrapolating the semicircle to the Z'

(X axis), and the Nyquist plot for all the glasses is given in Fig. 5. The calculated conductivity values are given in Table V. From Table V, it is clear that conductivity has increased from 10^{-8} S/cm for glass G1 to 10^{-6} S/cm for glass G5.

All the glasses in the series except glass G5 have a single semicircle with a straight polarization arm. The occurrence of this polarization arm indicates a diffusion-controlled process[57] or diffusion of the ions in the material. On the other hand, glass G5 displayed two semicircles that are distinct and dissimilar, suggesting the presence of some inhomogeneity within the glass. In SEM-EDS studies, some non-uniform surfaces were also observed for glass G5. In DSC, two different melting events were observed for the glasses G3, G4, and G5, although both G3 and G4 did not display two semi-circles in the studied frequency and temperature range. For the same reason, we studied glass G5 in detail. As mentioned previously, the first semicircle corresponds to the charge transfer resistance, which is related to the diffusion of ions or electrons in the material. This charge transfer resistance arises due to the movement of charged species between the material and the electrode. The second semicircle can arise due to the presence of in-homogeneities/phase separation in the material, such as defects, impurities, or different phases. These in-homogeneities can introduce additional resistances and capacitances in parallel with the charge transfer resistance, which can contribute to the appearance of the second semicircle. The presence of two semicircles that are distinct and dissimilar in glass G5 also represent two separate relaxation processes within the glass.[86,88] Each process has its own relaxation time, which refers to the time it takes for the material to return to its original state after being subjected to a perturbation. As the temperature increases, the size of these semicircular arcs decreases. To correlate the impedance response of the samples under consideration, an electric circuit model consisting of a series of two resistors (R) and constant phase elements (CPE) was used to fit the experimental results. R-CPE denotes a resistor R in parallel connection with a constant phase element CPE,[8,86,89] and this circuit is commonly used to describe one semicircle in the impedance response of materials.[86] Taking into account the phenomena that emerge at the interfacial areas and are related to inhomogeneity and diffusion processes in the studied material,[87,90] the CPE has been introduced to accommodate the non-ideal Debye-like

TABLE V. Compositional dependence of conductivity (σ) (S/cm) for all temperatures.

| Temperature (°)C | Conductivity (S/cm) (σ) | | | | G5 | |
	G1	G2	G3	G4	σ at R_1	σ at R_2
30	…	…	…	2.03×10^{-8}	5.91×10^{-7}	…
40	…	…	…	4.39×10^{-8}	3.85×10^{-7}	5.45×10^{-9}
50	…	…	…	6.70×10^{-8}	3.26×10^{-7}	5.77×10^{-9}
60	…	…	3.90×10^{-8}	9.63×10^{-8}	…	…
70	…	…	6.80×10^{-8}	1.51×10^{-7}	1.36×10^{-6}	5.94×10^{-8}
80	…	…	1.17×10^{-7}	3.22×10^{-7}	1.81×10^{-6}	8.66×10^{-8}
90	…	2.36×10^{-8}	2.00×10^{-7}	5.19×10^{-7}	2.51×10^{-6}	1.40×10^{-7}
100	1.04×10^{-8}	3.08×10^{-8}	3.35×10^{-7}	8.47×10^{-7}	3.53×10^{-6}	1.48×10^{-7}

TABLE VI. Parameters R_1 (resistance from the boundary surface between different phases), R_2 (resistance of the amorphous phase), Q_1 and Q_2 (capacitance of the dispersive element), m (deviation parameter for indicating homogeneity), and τ (relaxation time) derived from impedance spectra analysis for glass G5 for selected temperatures.

T (°C)	R_1 (Ω)	R_2 (Ω)	Q_1 (nF)	Q_2 (pF)	m_1	m_2	τ_1 (μs)	τ_2 (ms)
70	2 115 700	86 137	4.32	437	0.8431	0.7954	10.97	46.37
80	1 486 500	64 086	4.14	470	0.8576	0.7944	7.17	37.91
90	921 550	46 324	3.69	563	0.8783	0.7865	3.87	33.18
100	872 090	32 803	3.77	605	0.8786	0.7853	3.74	25.23

behavior of the capacitance.[86,89,91] The CPE is a general form of a capacitor, which represents a power-law dependence on frequency in the impedance response. The impedance of a CPE element is defined by the relation given in Eq. (8),[86,89]

$$Z_{CPE} = Q^{-1} \times (j\omega)^{-m}, \qquad (8)$$

where ω is the angular frequency, whereas Q and m ($0 < m < 1$) are parameters whose values are determined by fitting the data. The impedance's magnitude or strength is determined by the constant

value Q. It represents how much the CPE element resists the current. The value of m determines the phase behavior of the CPE element. It determines whether the CPE element behaves as a capacitor ($m < 0$), resistor ($m = 0$), or inductor ($m > 0$). The impedance of the CPE element can be determined by varying the values of ω, Q, and m. Fitted parameters for glass G5 are given in Table VI. The fitted spectra for glass G5 for temperature (70–100 °C) are given in Fig. 6 and for (30–50 °C) are given in Fig. S8 in the supplementary material. From Fig. 6, it can be observed that the second semicircle becomes more pronounced
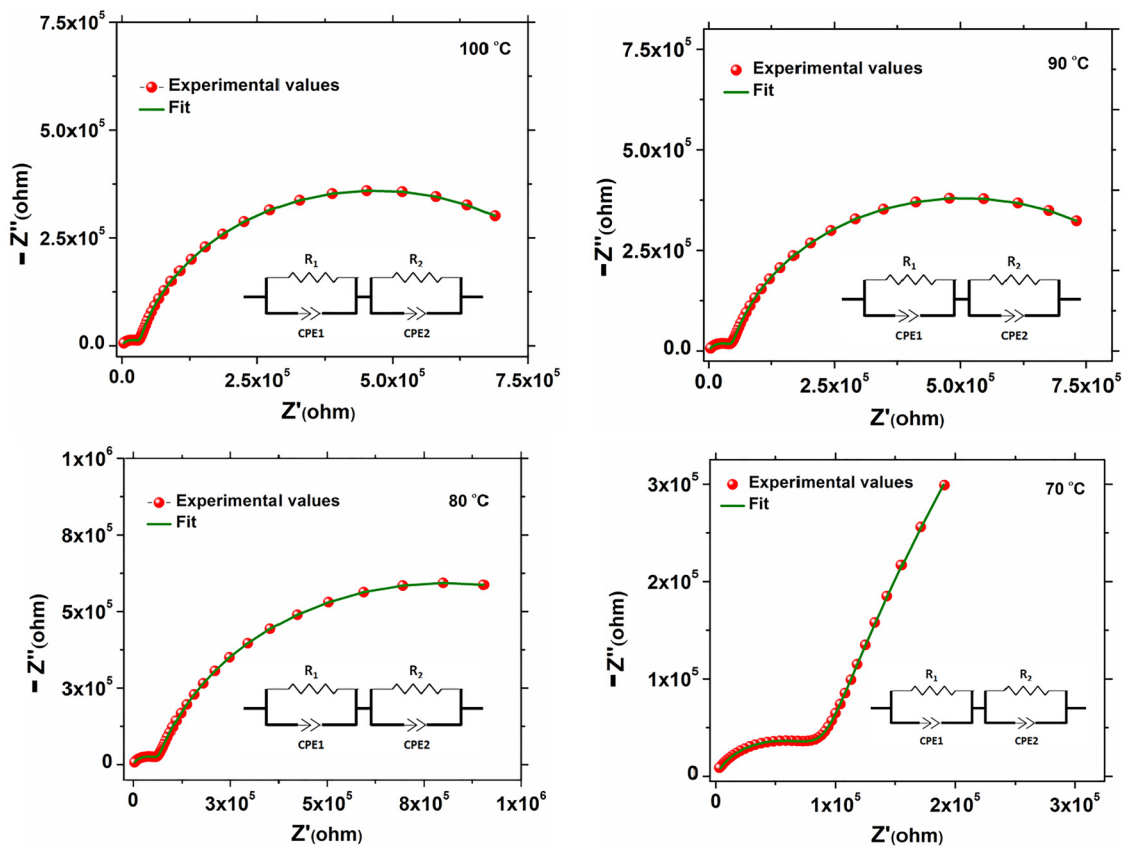

FIG. 6. Fitted (green lines) and experimental (scatter) impedance spectra for glass G5 from 70 to 100 °C. The inset shows the equivalent circuit model used for data analysis (R_1 and R_2: resistor and CPE1 and CPE2: constant phase element).

09 April 2024 09:31:30

with an increase in temperature from 30 to 50 °C. Figure 6 shows that there is a satisfactory agreement between the fitted (line) and experimental (scatter) data. The fitting errors for all the parameters were lower than 3%. Using estimated values of parameters R, Q, and m, the relaxation time was calculated by expression $\tau = (R \cdot Q) 1/m$,[86,92] and they are also listed in Table VI. Conductivity calculated from fitted spectra of glass G5 is given in Table V. The significant decrease of parameters R_1 and R_2 as a function of temperature corresponds to an increase in AC conductivity. It also signifies a shift of the valence band toward the Fermi level.[86,93,94] It is caused by the occurrence of defects generated by the presence of silver atoms and the partially ionic nature of Ag–S chemical bonds in the studied glass system.[95] From Table VI, it can be observed that the value of dispersive element Q_1 is higher compared to that of Q_2, which indicates that there is intense accumulation of charge carriers at the boundaries of separated phases, which relaxes at a lower frequency range.[8] The lower values of m_1 and m_2 indicate that

there is a certain level of inhomogeneity in the glass structure.[8] There is a sharp decrease in the relaxation time (τ) with an increase in temperature. Because chalcogenide glasses are semiconductors, it is expected that with an increase in temperature, the resistance should decrease, thus increasing the conductivity. The relaxation time also decreases as a function of temperature, signifying an increase in the dynamics of the relaxation processes.[88,96]

1. Frequency dependence of AC conductivity

The frequency dependence of AC conductivity for glass G5 from 30 to 100 °C is given in Fig. 7(a). From Fig. 7(a), the increase in AC conductivity is evident from room temperature to 100 °C. In the AC (alternating current) regime, the amorphous semiconductors such as chalcogenide glasses show dependence on temperature and frequency.[8] In amorphous semiconductors, the variations in AC conductivity with frequency at different temperatures obey the
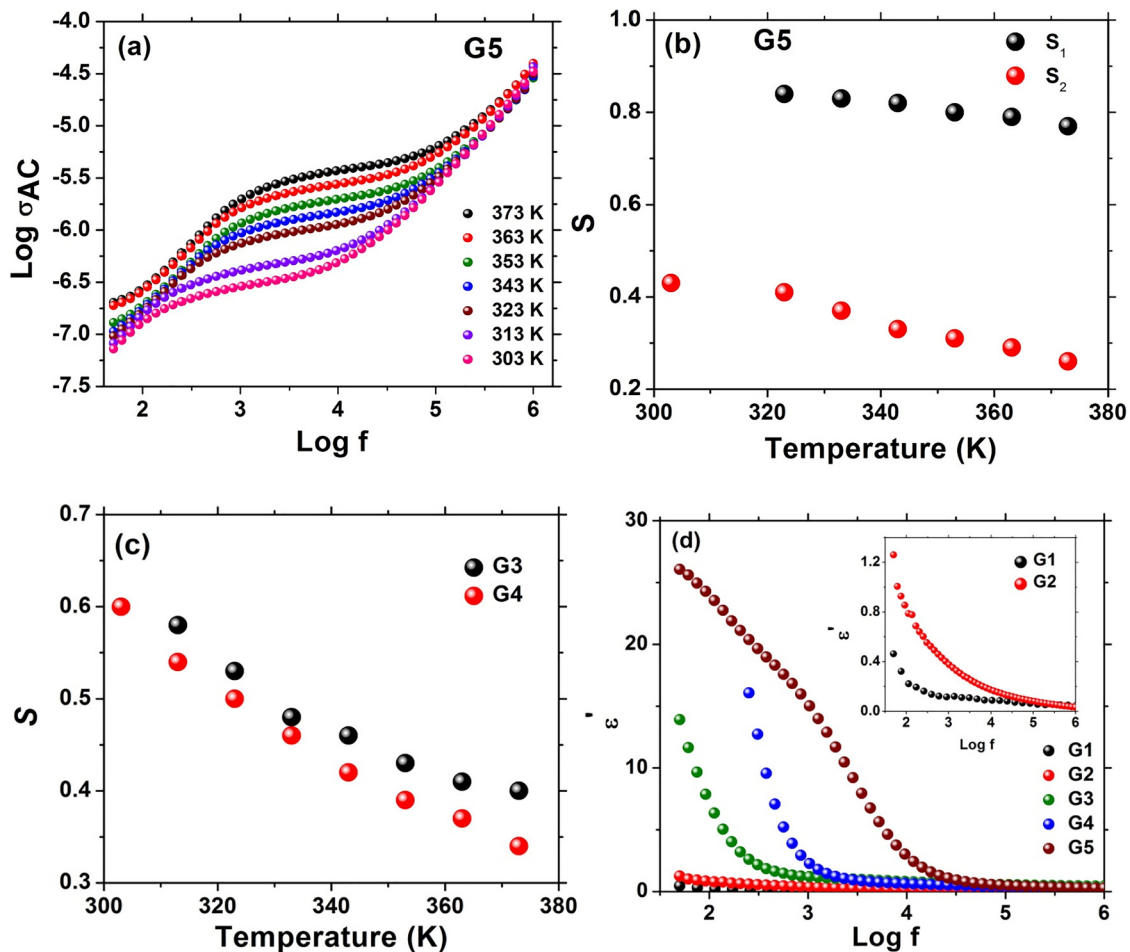
FIG. 7. (a) Frequency dependence of log σAc conductivity for glass G5. (b) Temperature dependence of the Jonscher parameter (s1) for the lower frequency region and (s2) for the higher frequency region for glass G5. (c) Jonscher parameters s for glasses G3 and G4. (d)Variation of dielectric constant for all studied glasses at 373 K (inset: dielectric constant variation for glasses G1 and G2).
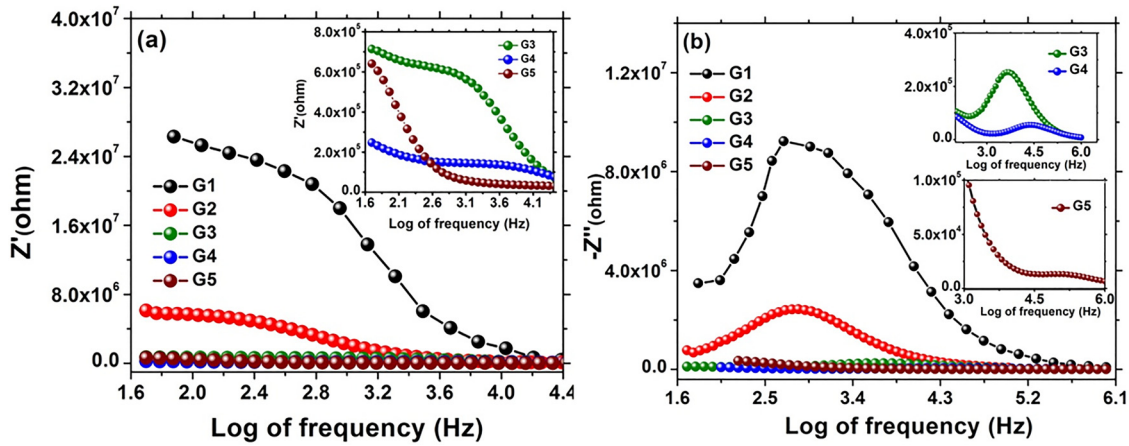
FIG. 8. The variation of (a) the real part (inset: magnified view for glasses G3–G5) and (b) imaginary part (inset: magnified view for glasses G3–G5) with frequency for all the studied compositions at 100 °C.

power law given by the empirical formula proposed by Jonscher and co-workers[8,96–98] and are given in Eq. (9),

$$\sigma_{AC}(\omega, T) = A(T) \times \omega^{S(T)}, \tag{9}$$

where ω is the angular frequency of the AC field, $A(T)$ is a function of temperature, and s ($0 \leq s \leq 1$) is Jonscher's parameter, which is dimensionless.

In the present study, the values of s were calculated from the slope of $\log(\sigma_{AC})$ vs log f for glass G5 from 30 to 100 °C and are given in Fig. 7(b). Based on the data presented in Fig. 7(b), it is evident that the values of Jonscher's coefficient decrease with increasing temperature, suggesting that there is an increase in the

potential barrier height.[96,99] In the case of glass G5, two distinct slopes are observed in the studied temperature range, suggesting the presence of two distinct mechanisms of conduction, as depicted in Fig. 7(a). This can be explained by using another term in Jonscher's empirical formula[8,96–98,100] and is given by Eq. (10),

$$\sigma_{AC}(\omega, T) = A(T) \times \omega^{s1(T)} + B(T) \times \omega^{s2(T)}, \tag{10}$$

where A and B are constants that are temperature-dependent, and s_1 and s_2 ($0 \leq s_{1,2} \leq 1$) are Jonscher's parameters. The temperature dependence of parameters s_1 and s_2 for the investigated samples is given in Fig. 7(b). The s parameter values decreased with an increase in temperature in glass G5. This behavior of s parameters is consistent
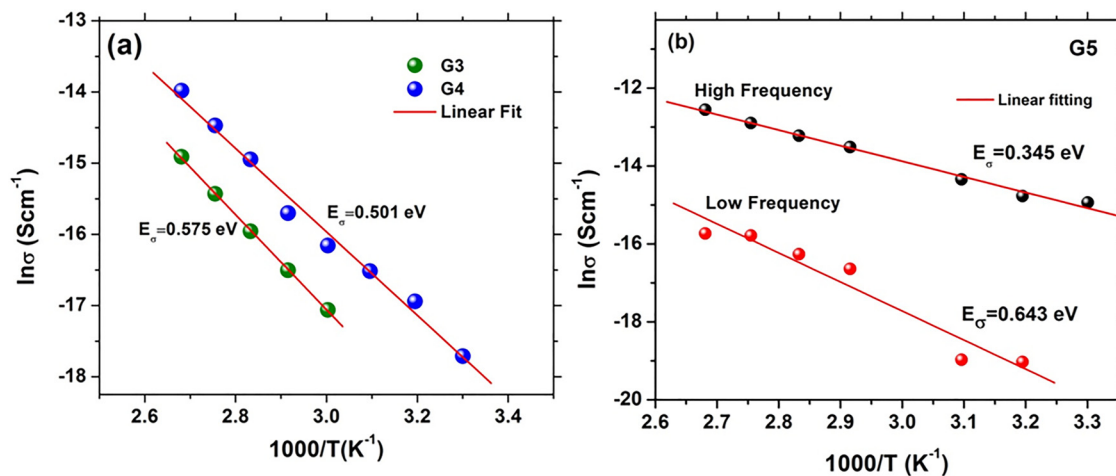

FIG. 9. Arrhenius plots for activation energies of (a) glasses G3 and G4. (b) Activation energies for both high and low frequency semicircular arcs in glass G5.

09 April 2024 09:31:30

with the correlated barrier hoping (CBH) model.[87,101] The AC conduction mechanism in the materials is described by the nature of the temperature dependence of Jonscher's coefficient s.[96,102] Generally, the temperature dependence of the frequency exponent s suggests that the CBH model proposed by Elliot[102] is appropriate for explaining the AC conduction mechanism in the studied glasses. As per this model, the AC conduction mechanism can be explained by the correlated barrier hopping of bipolarons, which occurs when two electrons simultaneously hop over a potential barrier between D^+ and D^-. The barrier height is related to the inter-site separation via Coulombic interaction.[96,103] Bipolaron hopping is the primary or dominant mechanism in the low and intermediate ranges due to the high diamagnetic defect states in those regions.[96,104] In the case of semiconductors, many theoretical models have been proposed to explain the parameter s. The s values for glass G3 and G4 are given in Fig. 7(c).

The dielectric constant ε' was determined by measuring the dielectric loss factor tanδ of the samples.[98,105] The dielectric constant was calculated by using Eq. (11),

$$\varepsilon' = \left(\frac{d}{\omega A \varepsilon_0} \times \frac{Z''}{Z'^2 + Z''^2).} \right) \qquad (11)$$

Here, d is the sample thickness, A is the area of the sample, ω is the angular frequency, Z' is the real part of impedance, Z'' is the imaginary part of impedance, and ε_0 is the vacuum permittivity.

The variation of the dielectric constant is shown in Fig. 7(d). As the amount of AgI in the samples increases, the dielectric constant also increases. Additionally, for all the samples, an increase in temperature leads to an increase in the dielectric constant. The dielectric constant is higher at lower frequencies and gradually decreases with an increase in frequency until it becomes almost constant. This can be attributed to the inability of the electric dipole to respond to changes in the applied electric field.

Furthermore, as the temperature increases, the magnitude of the dielectric constant also increases because more and more dipoles are able to align themselves along the field, resulting in a higher dielectric constant.[105,106] The variation of real and imaginary parts with the frequency at 100 °C for all the glasses is represented in Fig. 8. From Fig. 8(a), it is clearly seen that the real part Z′ decreases with an increase in silver iodide, indicating the enhancement in conductivity. The Z″ or imaginary part spectra of each glass [Fig. 8(b)] are characterized by the appearance of only one peak at a certain frequency f_{max} called the relaxation frequency. In all the glasses from G1 to G4, there is a single relaxation process as only one f_{max} is observed in the studied frequency range. However, in glass G5, it can be observed that there is the possibility of the appearance of another peak, indicating two relaxation processes. The activation energy for each sample was determined from the slope of the linear plots using the Arrhenius equation[8,86] and is given in Eq. (12),

$$\sigma_{AC} = \sigma_0 \times \exp\left(-\frac{E_\sigma}{K_B T} \right), \qquad (12)$$

where σ_0 is the pre-exponential factor, E_σ is the activation energy, K_B is the Boltzmann constant, and T is the temperature in kelvin.

Arrhenius plots for G3, G4, and G5 glasses are given in Fig. 9. A complete semicircle and polarization arm were observed only at 100 °C for G1 and from 80 to 100 °C for G2. For the same reason, no activation energies were calculated for G1 and G2. From Fig. 9(a), it is clear that activation energy started decreasing with an increase in the silver iodide content. Figure 9(b) shows activation energies at two different frequency regions for glass G5. The activation energy is two times greater at a higher frequency region compared to that of a lower frequency region. As per Ma et al.,[17] the linear nature of Arrhenius curves also indicates that conductivity is thermally activated. As per Lukić-Petrović et al.,[99] values of activation energy E_a represent the energy difference between the Fermi level and mobility gap edge, so the decrease in the activation energy can be interpreted as a consequence of the Fermi level shift toward the band of delocalized energy states. As per Lukić-Petrović et al.,[99] this occurs due to the existence of a higher number of defects in the more complex structures at an increased metal content and is also observed in the studied As–Sb–S–AgI glasses.

IV. CONCLUSION

The effect of replacing sulfur with silver iodide on structural, thermal, optical, mechanical, and electrical properties was investigated. The XRD analysis confirmed the amorphous nature of all the glasses, while the SEM-EDS analysis confirmed there was no loss in constituent elements, including iodine, in the final glass composition. Raman spectroscopy results indicate the formation of large numbers of As–I and Sb–I terminal bonds and enhancement in S–S–Ag or As–S–Ag bonds with an increase in AgI content. The structural changes in the glasses show an increase in AgI content, increased density, and electrical conductivity, while thermal and mechanical properties have shown a decline due to the increase in the formation of terminal bonds by iodine. The glasses have shown excellent transparency in the mid-infrared region, with the longer wavelength cutoff extending beyond 11 μm. Optical bandgap energies (E_g) have also shown that the glass with a higher silver iodide content has a wider optical bandgap energy. The increase in conductivity and simultaneous decrease in activation energy occurred with an increase in silver iodide concentration in the glass network. The non-uniform surface or inhomogeneity that was observed in SEM-EDS analysis of glass sample G5 was further confirmed by impedance spectroscopy as glass G5 displayed two unidentical semi-circles, indicating two different relaxation processes and also inhomogeneity present in the glass network. The nature of variation of AC conductivity is found to obey Jonscher's power law, and the values of exponent s suggest that the correlated barrier hopping model (CBH) is the most suitable model to characterize the electrical conduction mechanism of all prepared glasses. The dielectric constant ε' has shown an increase with an increase in AgI and also increased with an increase in temperature in every studied glass sample. The present research work also proved the importance of impedance spectroscopy in detecting inhomogeneity or clustering present in the glass.

SUPPLEMENTARY MATERIAL

The supplementary material presents the mole percent ratios of constituent elements from SEM-EDS data (Tables S1and S2),

SEM-EDS micrograph displaying inhomogeneity in glass G5 (Figs. S1–S4), DSC thermograms displaying melting events of glasses G1 and G2 (Fig. S5), deconvoluted Raman spectra (Fig. S6), basic chemical reaction of AgI with the As–Sb–S host glass (Fig. S7), and fitted impedance spectra for glass G5 (30–100 °C) (Fig. S8). All the explanation regarding supplementary figures and tables is explained in the manuscript itself.

AUTHOR DECLARATIONS

Conflict of Interest

The authors have no conflicts to disclose.

Author Contributions

Akila G. Prabhudessai: Conceptualization (equal); Data curation (equal); Formal analysis (equal); Investigation (equal); Methodology (equal); Visualization (equal); Writing – original draft (equal). **Sathravada Balaji:** Formal analysis (equal); Visualization (equal); Writing – review & editing (equal). **Sakthi Prasad:** Data curation (equal). **Shweta Chahal:** Data curation (equal); Methodology (equal). **Kaushik Biswas:** Formal analysis (equal); Investigation (equal); Writing – review & editing (equal). **K. Ramesh:** Visualization (equal); Writing – review & editing (equal). **Anupama Yadav:** Methodology (equal). **Saswata Chakraborty:** Data curation (equal). **Partha Sarathi Kongar:** Data curation (equal). **Sayan Chatterjee:** Data curation (equal). **Sutanu Dutta:** Data curation (equal). **Rana Dasgupta:** Methodology (equal). **Pratik Sarkar:** Methodology (equal). **K. Annapurna:** Conceptualization (equal); Formal analysis (equal); Funding acquisition (equal); Investigation (equal); Methodology (equal); Project administration (equal); Resources (equal); Supervision (equal); Validation (equal); Visualization (equal); Writing – review & editing (equal).

DATA AVAILABILITY

The data that support the findings of this study are available within the article and its supplementary material.

REFERENCES

[1] M. A. Popescu, *Non-Crystalline Chalcogenides* (Springer, Dordrecht, 2000).

[2] G. K. Ahluwalia, *Applications of Chalcogenides S, Se, and Te*, 1st ed. (Springer International Publishing, 2017).

[3] V. S. Shiryaev and M. F. Churbanov, *Chalcogenide Glasses* (Elsevier, 2014), pp. 3–35.

[4] T. Schweizer, "Rare-earth-doped gallium lanthanum sulphide glasses for mid-infrared fibre lasers," Ph.D. dissertation (Universität Hamburg, 1998).

[5] J. Hu, X. Sun, A. M. Agarwal, J.-F. Viens, L. C. Kimerling, L. Petit, N. Carlie, K. C. Richardson, T. Anderson, J. Choi, and M. Richardson, "Studies on structural, electrical, and optical properties of Cu doped As–Se–Te chalcogenide glasses," J. Appl. Phys. **101**(6), 063520 (2007).

[6] Z. Yang and P. Lucas, "Tellurium-based far-infrared transmitting glasses," J. Am. Ceram. Soc. **92**(12), 2920–2923 (2009).

[7] S. Cui, C. Boussard-Plédel, J. Lucas, and B. Bureau, "Te-based glass fiber for far-infrared biochemical sensing up to 16 μm," Opt. Express **22**(18), 21253 (2014).

[8] K. O. Čajko, D. L. Sekulić, D. M. Petrović, V. Labaš, S. Minárik, S. J. Rakić, and S. R. Lukić-Petrović, "Study of electrical and microstructural properties of Ag-doped As-S-Se chalcogenide glasses," J. Non-Cryst. Solids **571**, 121056 (2021).

[9] S. Cui, "Synthesis and characterization of tellurium based glasses for far infrared sensing and thermoelectric applications," Ph.D. dissertation (Université Rennes, 2014), p. 1.

[10] K. Michel, B. Bureau, C. Boussard-Plédel, T. Jouan, J. L. Adam, K. Staubmann, and T. Baumann, "Monitoring of pollutant in waste water by infrared spectroscopy using chalcogenide glass optical fibers," Sens. Actuators B **101**(1–2), 252–259 (2004).

[11] S. Danto, P. Houizot, C. Boussard-Pledel, X.-H. Zhang, F. Smektala, and J. Lucas, "A family of far-infrared-transmitting glasses in the Ga–Ge–Te system for space applications," Adv. Funct. Mater. **16**(14), 1847–1852 (2006).

[12] P. Wang, X. Wang, H. Guo, P. Zhang, S. Wang, S. Jia, G. Farrell, and S. Dai, *Mid-Infrared Fluoride and Chalcogenide Glasses and Fibers* (Springer Nature Singapore, Singapore, 2022).

[13] D. W. Hewak, D. Brady, R. J. Curry, G. Elliott, C.-C. Huang, M. Hughes, K. Knight, A. Mairaj, M. Petrovich, R. Simpson *et al.*, *Chalcogenide Glasses for Photonics Device Applications* (University of Southampton, 2010), pp. 29–102.

[14] C. Lin, E. Zhu, J. Wang, X. Zhao, F. Chen, and S. Dai, "Fast Ag-ion-conducting GeS$_2$–Sb$_2$S$_3$–AgI glassy electrolytes with exceptionally low activation energy," J. Phys. Chem. C **122**(3), 1486–1491 (2018).

[15] X. Huang, Q. Jiao, C. Lin, H. Ma, X. Zhang, E. Zhu, X. Liu, S. Dai, and T. Xu, "Formation, microstructure, and conductivity of a novel Ga$_2$S$_3$-Sb$_2$S$_3$-AgI chalcogenide system," Sci. Rep. **8**(1), 1699 (2018).

[16] X. Huang, Q. Jiao, C. Lin, Y. Zhang, Z. Yang, T. Xu, X. Zhang, H. Ma, X. Liu, and S. Dai, "Effect of heat treatment on AgI-rich chalcogenide glasses with enhanced ionic conductivity," J Am. Ceram. Soc. **102**(3), 1309–1315 (2019).

[17] B. Ma, Q. Jiao, Y. Zhang, C. Lin, X. Zhang, H. Ma, S. Dai, and G. Jia, "Conductivity and structural properties of fast Ag-ion-conducting GaGeSbS–AgI glassy electrolytes," Ceram. Int. **46**(16), 24882–24886 (2020).

[18] Q. Zhao, S. Stalin, C.-Z. Zhao, and L. A. Archer, "Designing solid-state electrolytes for safe, energy-dense batteries," Nat. Rev. Mater. **5**(3), 229–252 (2020).

[19] J. Ren, Q. Yan, T. Wagner, V. Zima, M. Frumar, B. Frumarova, and G. Chen, "Conductivity study on GeS$_2$-Ga$_2$S$_3$-AgI-Ag chalcohalide glasses," J. Appl. Phys. **114**(2), 023701 (2013).

[20] J. Saienga and S. W. Martin, "The comparative structure, properties, and ionic conductivity of LiI + Li$_2$S + GeS$_2$ glasses doped with Ga$_2$S$_3$ and La$_2$S$_3$," J. Non-Cryst. Solids **354**(14), 1475–1486 (2008).

[21] P. R. Rayavarapu, N. Sharma, V. K. Peterson, and S. Adams, "Variation in structure and Li+-ion migration in argyrodite-type Li$_6$PS$_5$X (X = Cl, Br, I) solid electrolytes," J. Solid State Electrochem. **16**(5), 1807–1813 (2012).

[22] S. Kondo, K. Takada, and Y. Yamamura, "New lithium ion conductors based on Li$_2$S-SiS$_2$ system," Solid State Ion. **53–56**, 1183–1186 (1992).

[23] D. S. Patil, M. S. Konale, J. Kolar, K. Shimakawa, V. Zima, and T. Wagner, "Ionic conductivity study of LiI-Ga$_2$S$_3$-GeS$_2$ chalcogenide glasses using a random-walk approach," Pure Appl. Chem. **87**(3), 249–259 (2015).

[24] J. E. Saienga, "Optimization of fast ionic conducting glasses for lithium batteries," Ph.D. dissertation (Iowa State University, Digital Repository, 2005).

[25]Y. Kim, J. Saienga, and S. W. Martin, "Anomalous ionic conductivity increase in $Li_2S + GeS2 + GeO_2$ glasses," J. Phys. Chem. B **110**(33), 16318–16325 (2006).

[26]Y. Zhang, Q. Jiao, B. Ma, X. Zhang, X. Liu, and S. Dai, "Effective ionic transport in AgI-based Ge(Ga)–Sb–S chalcogenide glasses," J. Am. Ceram. Soc. **102**(12), 7065–7070 (2019).

[27]J. Swenson and L. Börjesson, "Correlation between free volume and ionic conductivity in fast ion conducting glasses," Phys. Rev. Lett. **77**(17), 3569–3572 (1996).

[28]R. Zaiter, M. Kassem, D. Fontanari, A. Sokolov, T. Usuki, M. Bokova, A. C. Hannon, C. J. Benmore, F. Cousin, I. Ozheredov, and E. Bychkov, "Unexpected role of metal halides in a chalcogenide glass network," Mater. Des. **216**, 110547 (2022).

[29]H. Hoshino and M. Shimoji, "Electrical properties of silver iodide," J. Phys. Chem. Solids **35**(3), 321–326 (1974).

[30]S. Hoshino, "Crystal structure and phase transition of some metallic halides (IV) on the anomalous structure of α-AgI," J. Phys. Soc. Jpn. **13**(11), 1412A (1958).

[31]B. E. Mellander, "Electrical conductivity and activation volume of the solid electrolyte phase α-AgI and the high-pressure phase fcc AgI," Phys. Rev. B **26**(10), 5886–5896 (1982).

[32]R. D. Armstrong, R. S. Bulmer, and T. Dickinson, "Some factors responsible for high ionic conductivity in simple solid compounds," J. Solid State Chem. **8**(3), 219–228 (1973).

[33]M. Tatsumisago, Y. Shinkuma, and T. Minami, "Stabilization of superionic α-AgI at room temperature in a glass matrix," Nature **354**(6350), 217–218 (1991).

[34]B. Xu and X. Wang, "Thermally stable AgI quantum-dot-based room-temperature fast ionic conductors," Small **7**(24), 3439–3444 (2011).

[35]A. Taniguchi, M. Tatsumisago, and T. Minami, "Crystallization kinetics of α-AgI in Ag I-based silver orthoborate glasses," J. Am. Ceram. Soc. **78**(2), 460–464 (1995).

[36]M. Mroczkowska, "DSC and XRD studies on crystallization kinetics in AgI-rich glassy and glass-crystalline ionic conductors of the $AgI–Ag_2O–P_2O_5$ system," Solid State Ion. **179**(1–6), 202–205 (2008).

[37]J. G. P. Binner, G. Dimitrakis, D. M. Price, M. Reading, and B. Vaidhyanathan, "Hysteresis in the $\beta–\alpha$ phase transition in silver iodide," J. Therm. Anal. Calorim. **84**(2), 409–412 (2006).

[38]M. Marple, D. C. Kaseman, S. Kim, and S. Sen, "Superionic conduction of silver in homogeneous chalcogenide glasses," J. Mater. Chem. A **4**(3), 861–868 (2016).

[39]B. Ma, Q. Jiao, Y. Zhang, X. Sun, G. Yin, X. Zhang, H. Ma, X. Liu, and S. Dai, "Physical and electrochemical behaviors of AgX (X = S/I) in a $GeS_2–Sb_2S_3$ chalcogenide-glass matrix," Ceram. Int. **46**(5), 6544–6549 (2020).

[40]L. Li, S. Xu, H. Yin, Y. Wang, H. Zeng, and G. Chen, "Extended glass-forming region in the $AgCl-Ag_2S-As_2S_3$ ternary system," J. Am. Ceram. Soc. **101**(8), 3729–3738 (2018).

[41]L. Li, H. Yin, Y. Wang, J. Zheng, H. Zeng, and G. Chen, "A chalcohalide glass/alloy based Ag^+ ion—Selective electrode with nanomolar detection limit," Sci. Rep. **7**(1), 16752 (2017).

[42]G. Wang, C. Li, Q. Nie, Z. Pan, M. Li, Y. Xu, H. Wang, and D. Shi, "Thermal stability and far infrared transmitting property of $GeTe_4$-$AsTe_3$-AgI glasses and glass-ceramics," J. Non-Cryst. Solids **463**, 80–84 (2017).

[43]Y. V. Bobylev, E. A. Bychkov, and Y. S. Tver'yanovich, "Electrical properties of glasses in the $AgI-As_2Te_3$ system," Glass Phys. Chem. **30**(6), 519–522 (2004).

[44]M. Kassem, D. Le Coq, R. Boidin, and E. Bychkov, "New chalcogenide glasses in the $CdTe–AgI–As_2Te_3$ system," Mater. Res. Bull. **47**(2), 193–198 (2012).

[45]T. Usuki, S. Saito, K. Nakajima, O. Uemura, Y. Kameda, T. Kamiyama, and M. Sakurai, "Structural and electrical properties of AgI dispersed As-chalcogenide glasses," J. Non-Cryst. Solids **312–314**, 570–574 (2002).

[46]T. Usuki, K. Nakajima, T. Furukawa, M. Sakurai, S. Kohara, T. Nasu, Y. Amo, and Y. Kameda, "Structure of fast ion conducting $AgI–As_2Se_3$ glasses," J. Non-Cryst. Solids **353**(32–40), 3040–3044 (2007).

[47]E. I. Kamitsos, J. A. Kapoutsis, I. P. Culeac, and M. S. Iovu, "Structure and bonding in As−Sb−S chalcogenide glasses by infrared reflectance spectroscopy," J. Phys. Chem. B **101**(51), 11061–11067 (1997).

[48]K. White, R. L. Crane, and J. A. Snide, "Crystallization kinetics of As-Sb-S glass in bulk and thin film form," J. Non-Cryst. Solids **103**(2–3), 210–220 (1988).

[49]Y. M. Azhniuk, V. Stoyka, I. Petryshynets, V. M. Rubish, O. G. Guranich, A. V. Gomonnai, and D. R. T. Zahn, "SbSI nanocrystal formation in As–Sb–S–I glass under laser beam," Mater. Res. Bull. **47**(6), 1520–1522 (2012).

[50]Y. M. Azhniuk, A. Villabona, A. V. Gomonnai, V. M. Rubish, V. M. Marjan, O. O. Gomonnai, and D. R. T. Zahn, "Raman and AFM studies of $(As_2S_3)_{0.45}(SbSI)_{0.55}$ thin films and bulk glass," J. Non-Cryst. Solids **396–397**, 36–40 (2014).

[51]T. Kohoutek, T. Wágner, M. Vlček, M. Vlček, and M. Frumar, "Physico-chemical properties of spin-coated Ag–As–Sb–S films," J. Non-Cryst. Solids **351**(27–29), 2205–2209 (2005).

[52]A. G. Prabhudessai, K. Biswas, S. Balaji, R. Dasgupta, P. Sarkar, and K. Annapurna, "Role of iodine in broadening the optical window of As-Sb-S-I chalcogenide glass system," J. Non-Cryst. Solids **470**, 47–52 (2017).

[53]A. G. Prabhudessai, S. Balaji, K. Biswas, R. Dasgupta, P. Sarkar, and K. Annapurna, "Correlation between Raman spectroscopy and mechanical properties of As-Sb-S-I chalcogenide glasses," J. Non-Cryst. Solids **507**, 56–65 (2019).

[54]S. Stehlik, J. Kolar, M. Bartos, M. Vlcek, M. Frumar, V. Zima, and T. Wagner, "Conductivity in Ag–As–S(Se, Te) chalcogenide glasses," Solid State Ion. **181**(37–38), 1625–1630 (2010).

[55]S. Stehlik, J. Kolar, H. Haneda, I. Sakaguchi, M. Frumar, and T. Wagner, "Phase separation in chalcogenide glasses: The system AgAsSSe," Int. J. Appl. Glass Sci. **2**(4), 301–307 (2011).

[56]F. Kyriazis, A. Chrissanthopoulos, V. Dracopoulos, M. Krbal, T. Wagner, M. Frumar, and S. N. Yannopoulos, "Effect of silver doping on the structure and phase separation of sulfur-rich As–S glasses: Raman and SEM studies," J. Non-Cryst. Solids **355**(37–42), 2010–2014 (2009).

[57]T. C. Hasapis, K. S. Andrikopoulos, E. Hatzikraniotis, V. Dracopoulos, T. Wagner, S. N. Yannopoulos, and K. M. Paraskevopoulos, "Vibrational properties of silver-doped arsenic chalcogenide bulk glasses," AIP Conf. Proc **1203**, 283–288 (2010).

[58]A. Piarristeguy, M. Ramonda, N. Kuwata, A. Pradel, and M. Ribes, "Microstructure of Ag_2S-As_2S_3 glasses," Solid State Ion. **177**(35–36), 3157–3160 (2006).

[59]V. Balan, A. Piarristeguy, M. Ramonda, A. Pradel, and M. Ribes, "Phase separation and ionic conductivity: An electric force microscopy investigation of silver chalcogenide glasses," J. Optoelectron. Adv. Mater. **8**, 2112–2116 (2006), see https://old.joam.inoe.ro/arhiva/pdf8_6/6Balan.pdf

[60]J. Tauc, *Optical Properties of Amorphous Semiconductors: In Amorphous and Liquid Semiconductors* (Springer, Boston, MA, 1974), pp. 159–200.

[61]S.K. Tripathi, P.B. Barman, "Influence of composition on the optical band gap in a-$Ge_{20}Se_{80-x}In_x$ thin films," Chalcogenide Lett. **3**(12), 121 (2006), see http://www.ir.juit.ac.in:8080/jspui/bitstream/123456789/8749/1/Influence%20of%20composition%20on%20the%20optical%20band%20gap%20in%20A-Ge20Se80-XInX%20thin%20films.pdf.

[62]B. Ma, Q. Jiao, Y. Zhang, X. Sun, G. Yin, X. Zhang, H. Ma, X. Liu, and S. Dai, "Optimization of glass properties by substituting AgI with Ag_2S in chalcogenide system," Ceram. Int. **45**(17), 22694–22698 (2019).

[63]A. S. Bondarenko and G. A. Ragoisha, *EIS Spectrum Analyser, Beta version* (2008).

[64]X. Huang, Q. Jiao, C. Lin, T. Xu, H. Ma, X. Zhang, and S. Dai, "Compositional dependence of the optical properties of novel Ga-Sb-S-XI (XI = PbI_2,CsI, AgI) infrared chalcogenide glasses," J. Am. Ceram. Soc. **101**(2), 749–755 (2018).

[65]S. Cui, D. Le Coq, C. Boussard-Plédel, and B. Bureau, "Electrical and optical investigations in Te–Ge–Ag and Te–Ge–AgI chalcogenide glasses," J. Alloys Compd. **639**, 173–179 (2015).

[66]C. Cheng, X. Wang, T. Xu, L. Sun, Z. Pan, S. Liu, Q. Zhu, F. Liao, Q. Nie, S. Dai, X. Shen, X. Zhang, and W. Chen, "Optical properties of Ag- and AgI-doped Ge–Ga–Te far-infrared chalcogenide glasses," Infrared Phys. Technol. **76**, 698–703 (2016).

[67]M. Sakurai, F. Kakinuma, E. Matsubara, and K. Suzuki, "Partial structure analysis of amorphous $Ge_{15}Te_{80}M_5$ (M = Cu, Ag and In)," J. Non-Cryst. Solids **312–314**, 585–588 (2002).

09 April 2024 09:31:30

[68]K. A. Aly, "On the study of the optical constants for different compositions of Sn x (GeSe)$_{100-x}$ thin films in terms of the electronic polarizability, electronegativity and bulk modulus," Appl. Phys. A **120**(1), 293–299 (2015).

[69]M. N. Azlan, M. K. Halimah, S. Z. Shafinas, and W. M. Daud, "Electronic polarizability of zinc borotellurite glass system containing erbium nanoparticles," Mater. Exp. **5**(3), 211–218 (2015).

[70]Q. Guo, Y. Xu, H. Guo, X. Xiao, C. Lin, X. Cui, P. Wang, F. Gao, M. Lu, and B. Peng, "Effect of iodine (I$_2$) on structural, thermal and optical properties of Ge-Sb-S chalcohalide host glasses and ones doped with Dy," J. Non-Cryst. Solids **464**, 81–88 (2017).

[71]J. Heo and J. D. Mackenzie, "Chalcohalide glasses," J. Non-Cryst. Solids **111**(1), 29–35 (1989).

[72]M. Zhang, Z. Yang, H. Zhao, A. Yang, L. Li, and H. Tao, "Glass forming and properties of Ga$_2$S$_3$-Sb$_2$S$_3$-CsCl chalcohalide system," J. Alloys Compd. **722**, 166–172 (2017).

[73]V. M. Rubish, I. Yurkin, V. Malesh, V. Fedelesh, M. L. Trunov, and D. Semak, "Investigation of glass structure in As(Sb)-S(Se)-I systems by the methods of Raman spectroscopy and x-ray diffraction," SPIE **2648**, 530–536 (1995).

[74]V. M. Rubish, V. A. Stefanovich, P. P. Shtets, V. S. Gerasimenko, I. D. Turyanitsa, and V. Y. Slivka, "Vibrational spectra and structure of Sb$_x$S$_{1-x}$ glasses," J. Appl. Spectrosc. **52**(1), 36–39 (1990).

[75]L. Koudelka and M. Pisárčik, "Raman spectra and structure of As$_{40-x}$-S$_{60}$-I$_x$ glasses," Solid State Commun. **41**(1), 115–117 (1982).

[76]L. Koudelka and M. Pisárčik, "Raman spectra and structure of As-S-I system glasses," J. Non-Cryst. Solids **64**(1–2), 87–94 (1984).

[77]M. V. Kurushkin, V. A. Markov, A. V. Semencha, M. D. Mikhailov, A. S. Tverjanovich, A. L. Shakhmin, T. V. Larionova, and V. D. Andreeva, "Determination of AsSI-SbSI glasses short-range structure via Raman spectroscopy, XPS and XRD," Int. J. Appl. Glass Sci. **9**(1), 85–89 (2018).

[78]R. Holomb, V. Mitsa, P. Johansson, N. Mateleshko, A. Matic, and M. Veresh, "Energy-dependence of light-induced changes in g-As$_{45}$S$_{55}$ during recording the micro-Raman spectra," Chalcogenide Lett. **2**(7), 63–69 (2005), see https://dspace.uzhnu.edu.ua/jspui/bitstream/lib/4322/1/09_ChalcLett-2005.pdf.

[79]A. Douaud, S. H. Messaddeq, and Y. Messaddeq, "Photo-induced birefringence and surface ripples structures in As-S-Ag chalcogenide thin-films," J. Non-Cryst. Solids **519**, 119446 (2019).

[80]M. Ohta, "Effect of small amounts of silver on the electrical properties of As$_2$S$_3$ glasses," Phys. Status Solidi A **159**(2), 461–468 (1997).

[81]I. T. Penfold and P. S. Salmon, "Glass formation and short-range order in chalcogenide materials: The (Ag$_2$S)$_x$(As$_2$S$_3$)$_{1-x(0 \leq x \leq 1)}$ pseudobinary tie line," Phys. Rev. Lett. **64**(18), 2164–2167 (1990).

[82]A. Bertoluzza, C. Fagnano, P. Monti, and G. Semerano, "Raman and infrared spectra of As$_2$S$_x$ chalcogenide glasses with x $\leqslant$ 3," J. Non-Cryst. Solids **29**(1), 49–60 (1978).

[83]J. Tasseva, R. Todorov, T. Babeva, and K. Petkov, "Structural and optical characterization of Ag photo-doped thin As$_{40}$S$_{60-x}$Se$_x$ films for non-linear applications," J. Opt. **12**(6), 065601 (2010).

[84]A. Kannappan, S. Thirumaran, and R. Palani, "Elastic and mechanical properties of glass specimen by ultrasonic method," ARPN J. Eng. Appl. Sci. **4**(1), 27–31 (2009), see https://citeseerx.ist.psu.edu/document?repid=rep1&type=pdf&doi=576e51b032391fe069565e6c26dea60ca7f7d9dd.

[85]M. K. Halimah, A. A. A. Sidek, W. M. Daud, H. Zainul, Z. A. Talib, A. W. Zaidan, and H. Mansor, "Ultrasonic study and physical properties of borotellurite glasses," Am. J. Appl. Sci. **2**(11), 1541–1546 (2005).

[86]M. V. Šiljegović, S. R. Lukić Petrović, D. L. Sekulić, G. R. Štrbac, F. Skuban, O. Bošák, and D. M. Petrović, "Investigation of thermal and electrical properties of As–Se glasses modified with Cu using DSC and AC impedance spectroscopy," Appl. Phys. A **124**(12), 858 (2018).

[87]J. R. Macdonald and W. B. Johnson, *Fundamentals of Impedance Spectroscopy Impedance Spectroscopy* (John Wiley & Sons, Inc., 2018), pp. 1–20.

[88]M. Younas, M. Nadeem, M. Atif, and R. Grossinger, "Metal-semiconductor transition in NiFe$_2$O$_4$ nanoparticles due to reverse cationic distribution by impedance spectroscopy," J. Appl. Phys. **109**(9), 093704 (2011).

[89]F. D. Morrison, D. J. Jung, and J. F. Scott, "Constant-phase-element (CPE) modeling of ferroelectric random-access memory lead zirconate-titanate (PZT) capacitors," J. Appl. Phys. **101**(9), 094112 (2007).

[90]E. J. Abram, D. C. Sinclair, and A. R. West, "A strategy for analysis and modelling of impedance spectroscopy data of electroceramics: Doped lanthanum gallate," J. Electroceramics **10**(3), 165–177 (2003).

[91]J. Drechsel, B. Männig, D. Gebeyehu, M. Pfeiffer, K. Leo, and H. Hoppe, "MIP-type organic solar cells incorporating phthalocyanine/fullerene mixed layers and doped wide-gap transport layers," Org. Electron. **5**(4), 175–186 (2004).

[92]R. Martínez, A. Kumar, R. Palai, J. F. Scott, and R. S. Katiyar, "Impedance spectroscopy analysis of Ba$_{0.7}$Sr$_{0.3}$TiO$_3$/La$_{0.7}$Sr$_{0.3}$MnO$_3$ heterostructure," J. Phys. D: Appl. Phys. **44**(10), 105302 (2011).

[93]M. Kitao, H. Akao, T. Ishikawa, and S. Yamada, "Influence of copper addition on electrical and optical properties of amorphous As$_2$Se$_3$," Phys. Status Solidi A **64**(2), 493–498 (1981).

[94]Y. Sawan, M. El-Gabaly, A. Katrib, and M. Abu-Zeid, "Electronic band structure in the ternary system As-Se-Cu," J. Non-Cryst. Solids **59–60**, 1027–1030 (1983).

[95]M. A. Afifi, H. H. Labib, M. H. El-Fazary, and M. Fadel, "Electrical and thermal properties of chalcogenide glass system Se$_{75}$Ge$_{25-x}$Sb$_x$," Appl. Phys. A **55**(2), 167–169 (1992).

[96]K. O. Čajko, D. L. Sekulić, S. Lukić-Petrović, M. V. Šiljegović, and D. M. Petrović, "Temperature-dependent electrical properties and impedance response of amorphous Ag$_x$(As$_{40}$-S$_{30}$-Se$_{30}$)$_{100-x}$ chalcogenide glasses," J. Mater. Sci. Mater. Electron. **28**(1), 120–128 (2017).

[97]A. K. Jonscher, "The 'universal' dielectric response," Nature **267**(5613), 673–679 (1977).

[98]S. Singh, S. C. Katyal, and N. Goswami, "Dielectric and electrical study of zinc copper ferrite nanoparticles prepared by exploding wire technique," Appl. Phys. A **125**(9), 638 (2019).

[99]S. R. Lukić-Petrović, F. Skuban, D. M. Petrović, and M. Slankamenac, "Effect of copper on DC and AC conductivities of (As$_2$Se$_3$)–(AsI$_3$) glassy semiconductors," J. Non-Cryst. Solids **356**(44–49), 2409–2413 (2010).

[100]G. Yellaiah, T. Shekharam, K. Hadasa, and M. Nagabhushanam, "Low temperature DC conductivity, impedance spectroscopy and dielectric properties of Na doped Cd$_{0.8}$Zn$_{0.2}$S semiconductor compounds," J. Alloys Compd. **609**, 192–200 (2014).

[101]S. R. Elliott, "A theory of a.c.: Conduction in chalcogenide glasses," Philos. Mag. **36**(6), 1291–1304 (1977).

[102]D. L. Sekulic, Z. Z. Lazarevic, M. V. Sataric, C. D. Jovalekic, and N. Z. Romcevic, "Temperature-dependent complex impedance, electrical conductivity and dielectric studies of MFe$_2$O$_4$ (M = Mn, Ni, Zn) ferrites prepared by sintering of mechanochemical synthesized nanopowders," J. Mater Sci. Mater. Electron. **26**(3), 1291–1303 (2015).

[103]H. E. Atyia, "Electrical conductivity and dielectric relaxation of bulk Se$_{70}$Bi$_{(30-x)}$Te$_x$, x=(0, 15) chalcogenide glasses," J. Non-Cryst. Solids **391**, 83–90 (2014).

[104]A. Sharma, A. Kumar, and N. Mehta, "Determination of density of defect states in glassy Se$_{98}$M$_2$ (M = Ag, Cd and Sn) alloys using a.c.: Conductivity measurements," Measurement **75**, 69–75 (2015).

[105]J. H. Joshi, D. K. Kanchan, M. J. Joshi, H. O. Jethva, and K. D. Parikh, "Dielectric relaxation, complex impedance and modulus spectroscopic studies of mix phase rod like cobalt sulfide nanoparticles," Mater. Res. Bull. **93**, 63–73 (2017).

[106]K. Somashekhara Udupa, P. Mohan Rao, S. Aithal, A. P. Bhat, and D. K. Avasthi, "Effect of heavy-ion irradiation on dielectric constant and electrical conductivity of doped and undoped nonlinear substance," Bull. Mater. Sci. **20**(8), 1069–1077 (1997).

09 April 2024 09:31:30